Entropy generation analysisfor the design optimizationof solid oxide fuel cells

Cite this article as: Sciacovelli A, Verda V, Entropy generation analysis for the design optimization of solid oxide fuel cells International Journal of Numerical Methods for Heat & Fluid Flow Vol. 21 No. 5, 2011 . 535-558, DOI 10.1108/09615531111135819

ENTROPY GENERATION ANALYSIS FOR THE DESIGN OPTIMIZATION OF SOLID OXIDE FUEL CELLS

Abstract

Purpose - The aim of this paper is to investigate performance improvements of a monolithic solid oxide fuel cell geometry through an entropy generation analysis.

Design/methodology/approach – The analysis of entropy generation rates makes it possible to identify the phenomena that cause the main irreversibilities in the fuel cell, to understand their causes and to propose changes in the design and operation of the system. The various contributions to entropy generation are analyzed separately in order to identify which geometrical parameters should be considered as the independent variables in the optimization procedure. The local entropy generation rates are obtained through 3D numerical calculations, which account for the heat, mass, momentum, species and current transport. The system is then optimized in order to minimize the overall entropy generation and increase efficiency.

Findings – In the optimized geometry the power density is increased by about 10% compared to typical designs. In addition, a 20 % reduction in the fuel cell volume can be achieved with less than a 1% reduction in the power density with respect to the optimal design.

Research limitations/implications – The physical model is based on a simple composition of the reactants, which also implies that no chemical reactions (water gas shift, methane steam reforming, etc.) take place in the fuel cell. Nevertheless, the entire procedure could be applied in the case of different gas compositions.

Practical implications – Entropy generation analysis allows one to identify the geometrical parameters that are expected to play important roles in the optimization process and thus to reduce the free independent variables that have to be considered. This information may also be used for design improvement purposes.

Originality/value – In this paper, entropy generation analysis is used for a multi-physics problem that involves various irreversible terms, with the double use of this physical quantity: as a guide to select the most relevant design geometrical quantities to be modified and as objective function to be minimized in the optimization process.

Nomenclature

a	Surface absorption coefficient
$\vec{g}$	Gravitation field (m s^{-2})
h	Specific enthalpy (J kg^{-1})
$I(\vec{r},\vec{s})$	Radiation Intensity (W m^{-2} Sr^{-1})
$\vec{J}_i$	Diffusive flux of species *i* (kg m^{-2} s^{-1})
$\vec{J}_q$	Heat flux (W m^{-2})
K	Permeability (m^2)

Cite this article as: Sciacovelli A, Verda V, Entropy generation analysis for the design optimization of solid oxide fuel cells International Journal of Numerical Methods for Heat & Fluid Flow Vol. 21 No. 5, 2011 . 535-558, **DOI 10.1108/09615531111135819**

k	Thermal conductivity (W m^{-1} K^{-1})
p	Pressure (Pa)
R	Universal gas constant (W mol^{-1} K^{-1})
S_i	Species source term (kg m^{-3} s^{-1})
S_h	Heat source term (W m^{-3} s^{-1})
s_i	Specific entropy of species *i*
G_p	Total entropy generation (W K^{-1})
g_p	Total entropy generation per unit volume (W m^{-3} K^{-1})
T	Temperature (K)
$\vec{V}$	Velocity vector (m s^{-1})
V	Voltage (V)

Greek symbols

$\Phi(\vec{s}_i, \vec{s})$	Phase function (W m^{-2} Sr^{-1})
φ	Potential (V)
β	Transfer coefficient
Δ	Strain tensor (s^{-1})
ε	porosity
μ	Viscosity (m s^{-2})
μ_i	Chemical potential of species *i*

Cite this article as: Sciacovelli A, Verda V, Entropy generation analysis for the design optimization of solid oxide fuel cells International Journal of Numerical Methods for Heat & Fluid Flow Vol. 21 No. 5, 2011 . 535-558, DOI 10.1108/09615531111135819

ρ	Density (kg m^{-3})
σ	Electric conductivity (Ω^{-1} m^{-1})
σ_b	Stefan-Boltzmann constant (W m^{-2} K^{-1})
σ_s	Scattering coefficient
$\vec{\sigma}$	Entropy flux
ω_i	Mass fraction of species *i*

Subscritpts

μ	Fluid friction entropy generation
h	Heat transfer entropy generation
m	Mass transfer entropy generation
c	Heat – mass transfer entropy generation
rad	Radiative heat transfer entropy generation

1. INTRODUCTION

One of the main advantages of high temperature fuel cells resides in their theoretical efficiency (Larminie and Dicks, 1999). Nevertheless, the registered efficiency in real plants is still far from the potential performance (NETL and DOE, 2004; Calì *et al.*, 2006). One of the causes of this discrepancy is related to the non-uniformities in thermodynamic quantities such as the temperatures, concentrations, mass flow rates, etc., that provoke inhomogeneous distributions in the current densities and power production. This cause is investigated in this paper, together with possible improvements that could be achieved by changing the fuel cell geometry. This kind of analysis is usually conducted using numerical models that are able to relate information concerning the geometry, materials and operating conditions, to the corresponding performances.

Fuel cell operation involves various interconnected physical phenomena: fluid flow, chemical and electrochemical reactions, heat transfer, current transfer. These phenomena take place at multiple scales, thus, proper hypotheses should be formulated to model them. Various numerical models, which differ according to the hypotheses and to the application, have been proposed in the literature. As far as solid oxide fuel cells (SOFC) are concerned, a comprehensive description of these models can be found in review papers and books (see, for example, Kakaç et al., 2007; Andersson et al., 2010, VV.AA., 2008). Here, only some specific aspects related to the tubular-derived monolithic geometry are briefly presented.

Cite this article as: Sciacovelli A, Verda V, Entropy generation analysis for the design optimization of solid oxide fuel cells International Journal of Numerical Methods for Heat & Fluid Flow Vol. 21 No. 5, 2011 . 535-558, DOI 10.1108/09615531111135819

In the case of a tubular geometry, a large number of mesh elements are generally necessary because of the large ratio between the length and thickness of the layers, which is of the order of 500-1000 [Hwang et al., 2005; VV.AA., 2005]. A second particular feature of such a geometrical configuration concerns the non negligible effects of radiation heat transfer in both the single cells [Haynes and Wepfer, 2001] and in the stacks [Verda and Borchiellini, 2007]. Commercial codes sometimes impose constraints to face these issues which oblige one to introduce some simplifications into the models. As an alternative, various studies have been conducted using non-commercial codes that are generally more flexible (see, for example, Arpino and Massarotti, 2009).

In the present paper, a fuel cell model has been implemented using the Fluent® commercial code. The model relates the distribution of quantities, such as the velocities, concentrations, temperatures, current densities etc., to the operating conditions, geometry and materials. Compared to the models that are usually adopted for SOFC, a great deal of effort has been made to account for thermal radiation in a proper way.

In order to identify the main causes of inefficiencies, the local distributions of the corresponding entropy generation terms have been calculated from the previously mentioned quantities. This picture is used to select the geometrical parameters that should be modified in order to optimize the fuel cell performances. These are evaluated on the basis of the global entropy generation (which is minimized) and the power density.

2. FUEL CELL MODEL

A tubular-like solid oxide fuel cell geometry, obtained considering a monolithic type fuel cell [Yang et al., 2007] with the addition of an air injection tube, is shown in Figure 1.

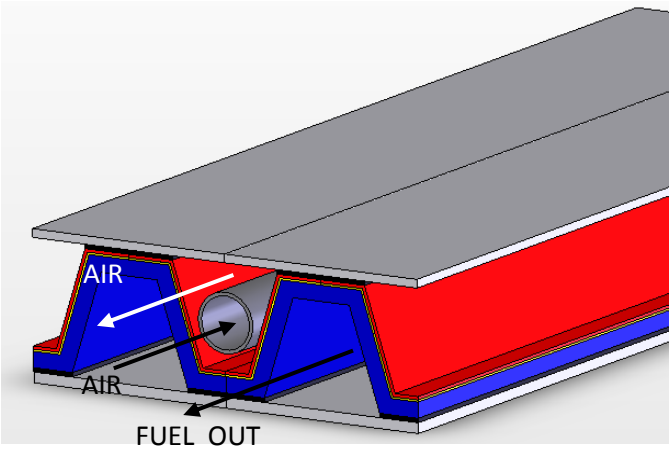

Figure 1. Schematic of fuel cell module

The fuel cell is composed of a solid electrolyte layer located between a porous cathode and a porous anode. There are two interconnections above and below this matrix. The fuel (a mixture of hydrogen and water vapour) and air flow in trapezoidal channels, but air is introduced through an injection tube located inside the cathodic channel. The air flows from the top of the cell to the bottom. When it reaches the bottom, it reverses the direction and flows in the trapezoidal air channels from the bottom to the top, in a co-current configuration with respect to the fuel flow. Table 1 shows details of the fuel cell geometry and model (Yang et al., 2007; Hwang et al., 2005; Li and Chyu, 2003).

This fuel cell is analyzed using a CFD model, which provides a detailed description of the physical phenomena that take place in fuel cells as well as the effect of the geometry of these phenomena. A three-dimensional CFD model that accounts for heat and mass transfer as well as chemical and electrochemical reactions is used.

Cite this article as: Sciacovelli A, Verda V, Entropy generation analysis for the design optimization of solid oxide fuel cells International Journal of Numerical Methods for Heat & Fluid Flow Vol. 21 No. 5, 2011 . 535-558, DOI 10.1108/09615531111135819

The model consists of 7 partial differential equations which are solved in each domain: continuity equation, momentum equation (3 components), energy equation, conservation of species and conservation of charge (Bird et al, 1960; VV.AA., 2008). The following hypotheses are considered: steady state conditions, the gas mixtures are modeled as an ideal gas, the fluid flow is laminar and incompressible, the porous electrodes are homogeneous and isotropic with uniform morphology proprieties (porosity, tortuosity and permeability), and thermal equilibrium is considered between the solid phase and the gas in the porous media.

Table 1. Geometrical parameters

Anode	Thickness (mm)	1.4
	Porosity	0.3
	Tortuosity	3
	Pore size (m)	$1\cdot10^{-6}$
	Permeability (m^2)	$1\cdot10^{-12}$
	Exchange current (A m^{-2})	$1\cdot10^{9}$
	Activation energy (J mol^{-1})	120
	Electrical conductivity (Ω^{-1} m^{-1})	$3.3\cdot10^{5}$
	Thermal conductivity (W m^{-1} K^{-1})	6.23
Cathode	Thickness (mm)	0.4
	Porosity	0.3
	Tortuosity	3
	Pore size (m)	$1\cdot10^{-6}$
	Permeability (m^2)	$1\cdot10^{-12}$
	Exchange current (A m^{-2})	$5\cdot10^{7}$
	Activation energy (J mol^{-1})	120
	Electrical conductivity (Ω^{-1} m^{-1})	$7.9\cdot10^{3}$
	Thermal conductivity (W m^{-1} K^{-1})	1.15
Electrolyte	Thickness (mm)	0.1
	Active length (mm)	17
	Electrical conductivity (Ω^{-1} m^{-1})	$20500\cdot\exp(-9030/T)$
	Thermal conductivity (W m^{-1} K^{-1})	2.2
Fuel channel	Length (mm)	100
	Cross section (mm^2)	90
Air channel	Length (mm)	100
	Cross section (mm^2)	80
Injection tube	Diameter (mm)	10

The fluid flow is modeled considering the Navier-Stokes equation together with the continuity equation in the gas channels:

$$\rho\cdot\vec{V}\cdot\nabla\vec{V}=-\nabla p-\nabla\cdot\mathbf{T}+\rho\vec{g} \quad (1)$$

$$\nabla\cdot\rho\vec{V}=0 \quad (2)$$

where ρ is the density, μ the viscosity, $\vec{V}$ the velocity vector and $\mathbf{T}$ the viscous stress tensor, that is $\mathbf{T}=-\mu\cdot\nabla\vec{V}+\nabla\vec{V}^{t}$.

The Navier-Stokes equation is substituted with the Brinkman-extended Darcy equation in the porous media:

Cite this article as: Sciacovelli A, Verda V, Entropy generation analysis for the design optimization of solid oxide fuel cells International Journal of Numerical Methods for Heat & Fluid Flow Vol. 21 No. 5, 2011 . 535-558, DOI 10.1108/09615531111135819

$$\rho \cdot \vec{V} \cdot \nabla \vec{V} = -\nabla p - \nabla \cdot \mathbf{T} - \frac{\mu}{K}\vec{V} + \rho\vec{g} \quad (3)$$

where *K* is the permeability of the porous media. This equation is recommended when a free flow and a flow in porous media occur, as it allows one to set the continuity of velocity, normal stress and shear stress at the interface [Nield and Bejan, 1999].

The conservation of species is written for all the gas species, except one. In this work, this equation is written for hydrogen on the anodic side and oxygen on the cathodic side. The mass fractions of the remaining species (water vapor on the anodic side and nitrogen on the cathodic side) are obtained from the continuity equation. For the i-th species, this equation is expressed as:

$$\nabla \cdot \rho \cdot \vec{V} \cdot \omega_i = -\nabla \cdot \vec{J}_i + S_i \quad (4)$$

Where ω_i is the mass fraction of component *i*, and $\vec{J}_i$ is the diffusion flux of species *i*:

$$\vec{J}_i = \rho D_{i,eff} \nabla \omega_i + \frac{\rho \omega_i}{M} - M \sum_j D_{j,eff} \nabla \omega_j - \nabla M \sum_j D_{j,eff} \omega_j \quad (5)$$

The first term on the right-hand side represents the Fick diffusion due to concentration gradients. The last three terms are the corrections necessary to enforce the Stefan-Maxwell equations for the multi-component diffusion term. The effects of porous media on the diffusion process are taken in account through modified binary diffusivities [Fuller et al., 1966; Yakabe et al., 2000].

The source term S_i can be used to account for the chemical and electrochemical reactions. There are no chemical reactions in this application as the fuel is only constituted by hydrogen and water vapor. The triple-phase boundaries (TPBs), i.e. the active sites where the pores, electronic conductor and ionic conductor coexist, are considered to be located at the interface between the electrodes and the electrolyte. For this reason, electrochemical reactions are accounted through proper boundary conditions. These reactions are:

$$\frac{1}{2}O_2 + 2e^- \rightarrow O^{2-} \quad (6)$$

$$H_2 + O^{2-} \rightarrow H_2O + 2e^- \quad (7)$$

Oxygen is reduced in the TPBs on the cathode side. Oxygen ions are transported through the electrolyte, and reach the TPBs on the anodic side. Here electrochemical reaction (7) takes place. This means that oxygen is consumed on the cathodic side and hydrogen is consumed and water is generated on the anodic side.

The heat transfer inside the SOFC includes various aspects such as convective heat transfer between the solid surfaces and the gas streams, and conductive heat transfer in the solid and porous structures. In order to obtain a temperature profile in the fuel cell domain, the energy equation, which is written in the following form, is solved:

Cite this article as: Sciacovelli A, Verda V, Entropy generation analysis for the design optimization of solid oxide fuel cells International Journal of Numerical Methods for Heat & Fluid Flow Vol. 21 No. 5, 2011 . 535-558, DOI 10.1108/09615531111135819

$$\nabla\cdot\left(\rho\vec{V}\left(h+\frac{v^2}{2}\right)\right)=\nabla\cdot\left(k_{eff}\nabla T-\sum_i h_i\cdot\vec{J}_i\right)+S_h \quad (8)$$

where h is the specific enthalpy of the mixture, and h_i is the specific enthalpy of the i-th species. The effective thermal k_{eff} conductivity is calculated assuming a local temperature equilibrium (LTE) between the gas and the porous matrix, therefore

$$k_{eff}=\varepsilon\cdot k_f+(1-\varepsilon)\,k_s \quad (9)$$

in which ε is the porosity, *s* stands for solid and *f* for the fluid (gas) phase. The source term S_h in the energy equation accounts for Joule heating due to ohmic resistance:

$$S_h=\sigma\,\nabla\phi\cdot\nabla\phi \quad (10)$$

The terms related to the reversible electrochemical reaction and that accounting for activation losses are set at the TPBs as boundary conditions.

Apart from heat conduction and convection, thermal radiation is also considered in this study. In some cases, this contribution is negligible, especially when a single isolated fuel cell is considered (see, for example, Li and Suzuki, 2004). An important exception is that of tubular solid oxide fuel cells, where a large radiation heat transfer between the cathode surface and the fresh air injection tube takes place. This effect is not negligible (Ota et al., 2003; Haynes and Wepfer, 2001) and the temperature profiles that are obtained considering or not considering it are significantly different (Fischer and Seume, 2006).

Modeling thermal radiation propagation in the general case of participating media requires the solution of the radiative transfer equation (RTE). An integro-differential equation should be solved numerically:

$$\frac{\partial I}{\partial s}=-\,(a+\sigma_s)\,I+a\frac{n^2\sigma T^4}{\pi}+\frac{\sigma_s}{4\pi}\int_0^{4\pi}I(\vec{s}_i)\cdot\Phi(\vec{s}_i,\vec{s})\cdot d\Omega_i \quad (11)$$

where $I(\vec{r},\vec{s})$ is the radiation intensity, which depends on position $\vec{r}$ and direction $\vec{s}$, a the surface absorption coefficient, σ_s the scattering coefficient, n the refractive index and $\Phi(\vec{s}_i,\vec{s})$ the phase function.

The discrete ordinate (DO) (Chui and G. D. Raithby, 1993) solves the RTE equation for a finite number of discrete solid angles, each associated with a direction vector $\vec{s}$. This approach is applicable for any optical thickness. When solid oxide fuel cells are analyzed, radiation fluxes emitted and reflected by the walls are considered, as well as their extinction and emission by the flowing gases. Air mainly consists of simple non-polar nitrogen and oxygen molecules and, therefore, is non-interacting (transparent) with thermal radiation at moderate pressures and the temperatures found

Cite this article as: Sciacovelli A, Verda V, Entropy generation analysis for the design optimization of solid oxide fuel cells International Journal of Numerical Methods for Heat & Fluid Flow Vol. 21 No. 5, 2011 . 535-558, DOI 10.1108/09615531111135819

in SOFCs (Modest, 2003). The analysis of fuel channels is more complicated due to the presence of H_2O. Nevertheless, Damm and Fedorov (2005) have shown that fuel can be treated as a transparent gas for typical SOFCs dimensions. Thus, surface-to-surface radiation exchange is the only radiative transfer mode considered in this paper. The fineness of the angular discretization has been appropriately chosen to guarantee a grid independent solution.

In order to couple radiation to the other heat transfer mechanisms, the divergence of the total radiative heat flux is added to the overall energy conservation equation as a heat sink,

$$S = -\nabla \cdot \vec{q}_r \quad (12)$$

The last equation to solve is the charge conservation:

$$\nabla \cdot \left(-\sigma \cdot \nabla \phi \right) = 0 \quad (13)$$

where σ is the electrical conductivity and ϕ the electronic/ionic potential. Once the potential has been calculated, the current density distribution is obtained using Ohm's law.

$$\vec{i} = -\sigma \cdot \nabla \phi \quad (14)$$

The SOFC unit shown in Figure 1 is characterized by a symmetrical structure with respect to the longitudinal mid-planes of the air and fuel channel. Thus, symmetry boundary conditions are imposed for all the partial differential equations along the two planes. In addition, specific conditions are assumed for the various domains.

Velocity $\vec{V}$, mass fractions ω_i, and temperature T are specified on the inlet cross-sections; the mass flows and velocity are set to zero at the channel walls. Continuity is imposed at the electrode/channel flow interface. Pressure is set equal to the ambient pressure on the outlet cross-sections. In these sections, the flow is assumed to be purely convective in both the energy equation and the conservation of species.

The outer surfaces of the electrodes are isolated, thus the normal heat flow, mass flow and electric flow are zero, that is

$$\vec{i} \cdot \vec{n} = 0 \quad (15)$$

$$-k \nabla T \cdot \vec{n} = 0 \quad (16)$$

$$\vec{J}_i \cdot \vec{n} = 0 \quad (17)$$

Electrochemical reactions are considered to occur at the interfaces between the electrode and the electrolyte, where proper boundary conditions should be specified. For the electrical problem, the current generation (Buttler-Volmer equation [Noren and Hoffman, 2005]) is set:

$$\vec{i} \cdot \vec{n} = j_0 \cdot \left(e^{\frac{\beta \cdot n_e \cdot F}{R \cdot T} \eta_{act}} - e^{-\frac{1-\beta \cdot n_e \cdot F}{R \cdot T} \eta_{act}} \right) \quad (18)$$

where η_{act} is the electrode overpotential, β and n_e are the transfer coefficient and the number of electrons participating in the reaction, respectively. In this study, β=0.5 and n_e = 4 (for the cathode) or n_e = 2 (for the anode). The exchange

Cite this article as: Sciacovelli A, Verda V, Entropy generation analysis for the design optimization of solid oxide fuel cells International Journal of Numerical Methods for Heat & Fluid Flow Vol. 21 No. 5, 2011 . 535-558, DOI 10.1108/09615531111135819

current density j_0 depends on the partial pressures of the mixture species and temperature [Costamagna et al., 2004]. At the anode side,

$$j_0 = \gamma_{an} \cdot \left(\frac{p_{H_2}}{p_{ref}} \right) \left(\frac{p_{H_2O}}{p_{ref}} \right) e^{-\frac{E_{a,an}}{R \cdot T}} \quad (19)$$

At the cathode side

$$j_0 = \gamma_{ca} \cdot \left(\frac{p_{O_2}}{p_{ref}} \right)^{0.25} e^{-\frac{E_{a,ca}}{R \cdot T}} \quad (20)$$

The activation loss can be quantified as:

$$\eta_{act} = V_{rev} - \left| \phi_{electrode} - \phi_{electrolyte} \right| \quad (21)$$

in which V_{rev} is the reversible potential between the electrode and the electrolyte, which can be computed with Nernst's equation:

$$V_{cell} = -\frac{\Delta G^0}{n_e \cdot F} + \frac{R \cdot T}{n_e \cdot F} \cdot \ln \left(\frac{p_{H_2} \cdot \sqrt{p_{O_2}}}{p_{H_2O}} \right) \quad (22)$$

As far as the thermal problem is concerned, the heat flux generated on the surface between the electrodes and electrolyte is

$$\vec{\varphi} \cdot \vec{n} = \frac{j}{2F} T \cdot \Delta S + j \cdot \eta_{act} \quad (23)$$

where $\vec{\varphi}$ is the heat flux. The boundary conditions for mass transport are set through Faraday's law, which expresses hydrogen consumption and water generation at the interface between the anode and electrolyte, namely

$$\overrightarrow{J_{H_2}} \cdot \vec{n} = \frac{\vec{i} \cdot \vec{n}}{2F} M_{H_2} \quad (24)$$

Cite this article as: Sciacovelli A, Verda V, Entropy generation analysis for the design optimization of solid oxide fuel cells International Journal of Numerical Methods for Heat & Fluid Flow Vol. 21 No. 5, 2011 . 535-558, DOI 10.1108/09615531111135819

$$\overrightarrow{J_{H_2O}} \cdot \vec{n} = \frac{\vec{i} \cdot \vec{n}}{2F} M_{H_2O} \quad (25)$$

while it expresses oxygen consumption on the interface between cathode and electrolyte, namely:

$$\overrightarrow{J_{O_2}} \cdot \vec{n} = \frac{\vec{i} \cdot \vec{n}}{4F} M_{O_2} \quad (26)$$

The values of the boundary conditions are shown in Table 2.

Table 2. Boundary conditions

Hydrogen mass flow rate (kg/s)	$1.19 \cdot 10^{-6}$
Oxygen mass flow rate (kg/s)	$2.98 \cdot 10^{-5}$
Fuel inlet temperature (K)	973
Inlet hydrogen mass fraction (anode side)	0.4752
Inlet water mass fraction (anode side)	0.5248
Inlet oxygen mass fraction (cathode side)	0.2329
Inlet nitrogen mass fraction (cathode side)	0.7671
Operating voltage (V)	0.7

The computational grid is depicted in Figure 2. An unstructured grid is used in the domain corresponding to the cathodic channel because of the curved boundary of the injection tube. The fuel channel is instead meshed with a structured grid. A structured grid with a refined mesh is adopted in the electrode domains, in the proximity of the electrode/electrolyte interface. Finally, a non-uniform cell size is adopted along the longitudinal axis of the fuel cell: a refined grid is used in proximity of the inlet and outlet sections of the injection tube. The grid consists of about 500,000 elements (cells).

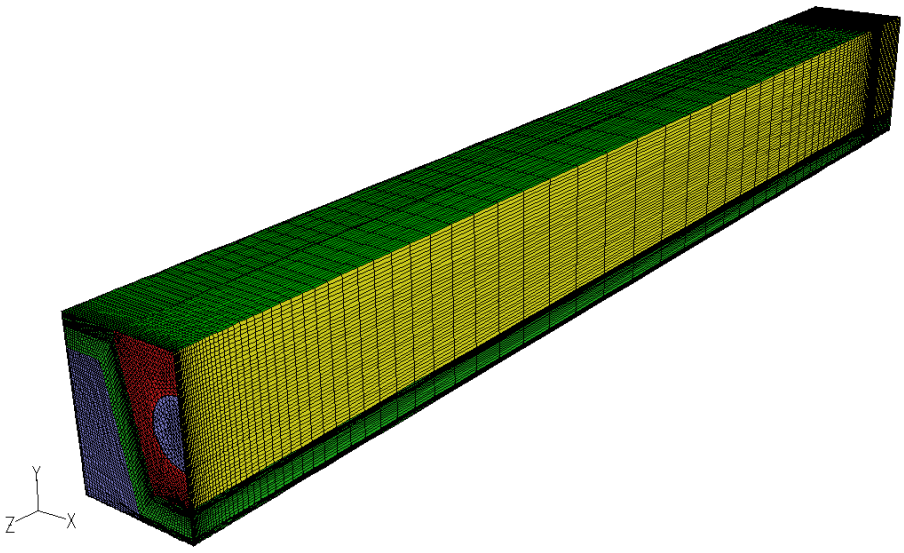

Figure 2. Computational grid.

The Navier–Stokes equation, transport equations and boundary conditions are discretized using the finite volume method (FVM) to obtain the velocity field, temperature and mass fractions in the fuel cell. The local current density is

Cite this article as: Sciacovelli A, Verda V, Entropy generation analysis for the design optimization of solid oxide fuel cells International Journal of Numerical Methods for Heat & Fluid Flow Vol. 21 No. 5, 2011 . 535-558, DOI 10.1108/09615531111135819

then computed and source terms for the species and energy equation are determined. This procedure is repeated until convergence is reached. Finally, the local and global entropy generation are calculated and stored. The convective terms in the equations are modeled using a second order upwind scheme, while the diffusive terms are modeled by means of a central difference scheme. The numerical solution procedure adopts the semi-implicit SIMPLE algorithm (Patankar, 1980). The convergence criterion has been set on the basis of the residuals on the continuity equation, which must be smaller than 10^{-6}. The residuals for the other equations are much smaller.

A validation of the proposed model through comparison with numerical results available in the literature is proposed in [Sciacovelli and Verda, 2009].

3. SIMULATION OF THE INITIAL FUEL CELL GEOMETRY

Figure 3 shows the velocity path lines inside the cathode channel. Air flows in the tube from the top of the cell to the bottom. Two vortexes occur at the closed end of the channel. This is typical of tubular fuel cells. Air flows back from the bottom to the top in the cathode channel. It is interesting to observe that the velocities are higher in the lower part of the channel; this is due to the smaller cross-section below the air tube.

The flow in the porous electrodes is mainly driven by diffusion phenomena: the net flow in the anode is directed towards the fuel channel. This is due to the production of water because of the electrochemical reaction. Oxygen is consumed on cathode side, thus the air flows from the channel to the cathode.

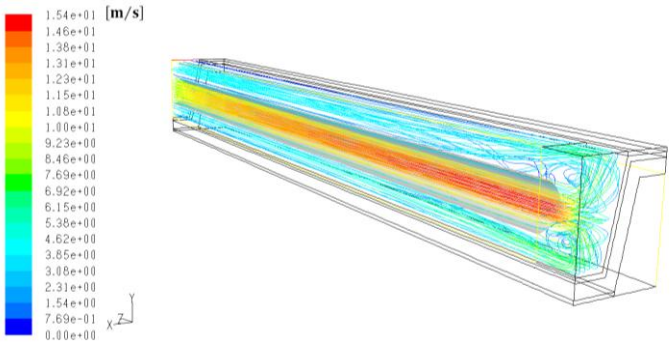

Figure 3. Velocity path lines inside cathode channel.

Figure 4 shows the hydrogen concentration in several transversal cross sections on the anode side. It is clear that the hydrogen mass fraction presents a strong gradient in streamwise directions, and this profile is characterized by the rate of consumption of the hydrogen due to electrochemical reactions. It is also evident that a concentration gradient occurs in the transversal direction. This is the result of the hydrogen diffusion process from the bulk flow to the three-phase boundary. This effect is stronger in the lower zone of the anode, where the hydrogen mass fraction is smaller.

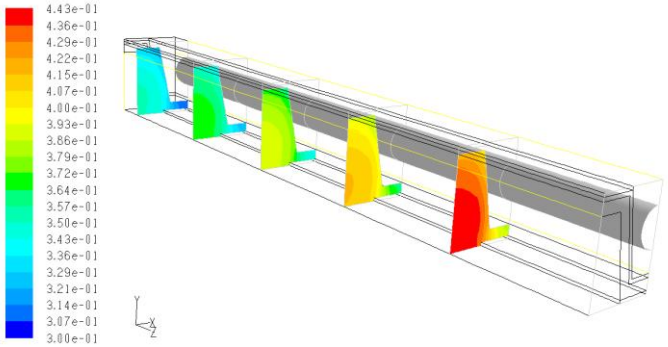

Figure 4. Distribution of hydrogen mass fraction.

Cite this article as: Sciacovelli A, Verda V, Entropy generation analysis for the design optimization of solid oxide fuel cells International Journal of Numerical Methods for Heat & Fluid Flow Vol. 21 No. 5, 2011 . 535-558, DOI 10.1108/09615531111135819

The oxygen mass fraction in the cathode channel is depicted in figure 5. Since air first flows inside the tube, the largest oxygen concentration is encountered in the bottom part of the cell. As in the hydrogen case, the oxygen mass fraction presents variations both in the streamwise direction and in the x-y plane. The oxygen cannot easily reach the upper plane of the cathode; this occurs because the porous matrix on the cathode side represents an obstacle to the air flow.

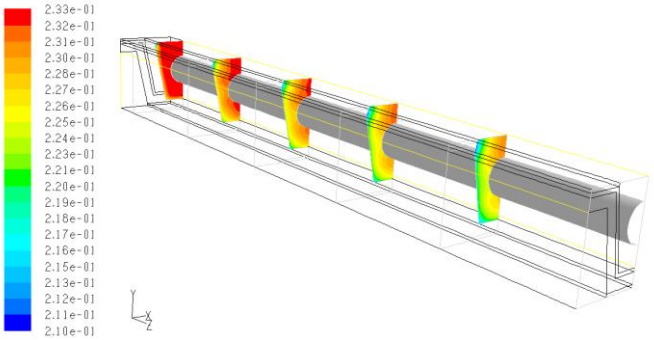

Figure 5. Oxygen mass fraction.

Figure 6 shows the temperature distribution in the fuel cell, without considering radiation.

Since the electrochemical reactions are exothermic, an overall increase in the cell temperature is expected with respect to the inlet conditions. However, the temperature distribution at the anode side shows different features from the cathode side. In the fuel channel, the temperature initially increases along the z direction and reaches a maximum value of 1063 K at 60% of the cell length, then the temperature decreases till the outlet section. In the cathode channel, instead, the outlet temperature is close to the inlet temperature. The air temperature increases monotonically from the outlet tube section to the inlet section.

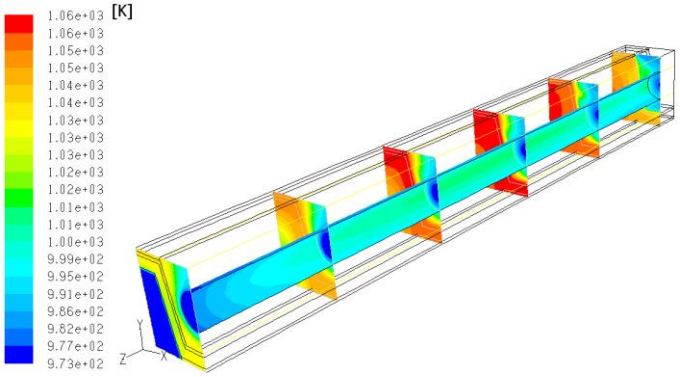

Figure 6. Temperature distribution without radiation.

It is interesting to notice that the temperature is much higher in the region below the air tube. There are significant temperature gradients along the cross sections, in particular in the electrodes. This is due to the limited convection in the porous matrix.

Figure 7 shows the temperature distribution obtained considering the radiation heat transfer. There are significant differences compared to the previous result. The injection tube temperature is higher, which also causes a higher temperature in the tube. Even more important, the pick temperature in the fuel cell is smaller because of the larger heat transfer.

Cite this article as: Sciacovelli A, Verda V, Entropy generation analysis for the design optimization of solid oxide fuel cells International Journal of Numerical Methods for Heat & Fluid Flow Vol. 21 No. 5, 2011 . 535-558, DOI 10.1108/09615531111135819

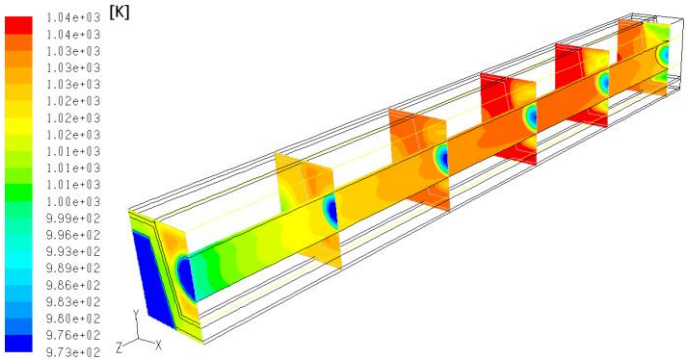

Figure 7. Temperature distribution with radiation heat transfer.

4. ENTROPY GENERATION ANALYSIS

The rate of entropy generation is used to chose the geometrical variables that should be used in the optimization procedure and then as the thermodynamic objective function to be minimized.

An expression of the entropy generation rate, in terms of fluxes, and the corresponding gradients of the physical quantities is used. This equation is obtained from the entropy balance, written for an infinitesimal volume, developed as an equation of change (Bejan, 1982):

$$\rho \cdot \frac{Ds}{Dt} = -\nabla \cdot \vec{\sigma} + g_p \quad (27)$$

where s is the entropy per unit mass, $\vec{\sigma}$ is the entropy-flux vector and g_p is the rate of entropy generation per unit volume. The entropy source g_p and the entropy flux may be calculated considering the Gibbs thermodynamic relation which, in an isotropic multi-component fluid, connects the entropy variation ds to the internal energy variation du and the variation in composition $d\omega_i$:

$$du = T \cdot ds - p \cdot d\left(\frac{1}{\rho}\right) + \sum_i \mu_i \cdot d\omega_i \quad (28)$$

where μ_i is the chemical potential of species i. Although the system is not in equilibrium, it is possible to assume that there is a state of local equilibrium within small mass elements. In particular, it is assumed that equation (28) remains valid for a mass element, which is followed along its centre of gravity motion:

$$\frac{Du}{Dt} = T \cdot \frac{Ds}{Dt} - p \cdot \frac{D}{Dt}\left(\frac{1}{\rho}\right) + \sum_i \mu_i \cdot \frac{D\omega_i}{Dt} \quad (29)$$

where D/Dt is the substantial derivative. The main purpose of this approach is to explicitly relate the entropy source to the various irreversible processes that occur in a system. Macroscopic conservation laws of mass, momentum and energy can be introduced to express the differentials in Eq. (29). After some rearrangement it is possible to show that [Hirschfelder et al., 1954]:

Cite this article as: Sciacovelli A, Verda V, Entropy generation analysis for the design optimization of solid oxide fuel cells International Journal of Numerical Methods for Heat & Fluid Flow Vol. 21 No. 5, 2011 . 535-558, DOI 10.1108/09615531111135819

$$\vec{\sigma} = \frac{1}{T}\left(\vec{J}_q + \sum_i \mu_i \vec{J}_i \right) \quad (30)$$

$$g_p = \frac{1}{T}\Delta : \mathbf{T} + \frac{1}{T^2} \; -\vec{J}_q \nabla T \; + \frac{1}{T}\sum_i -\vec{J}_i \cdot \nabla \mu_i + \frac{1}{T}\sum_i -s_i \vec{J}_i \cdot \nabla T \quad (31)$$

Equation (30) shows that, for open systems, the entropy flow consists of two parts: one is the reduced heat flow $\vec{J}_q / T$, the other is connected to the diffusion flows of matter $\vec{J}_k$. Equation (31) demonstrates that the entropy production contains various contributions. The first term on the right-hand side is connected to the velocity gradients, which originate from the viscous flow, the second term arises from heat conduction, the third from diffusion, and the fourth is due to coupling between the heat and the mass transfer (convective term). This means that the local rate of entropy generation is split into four main contributions, each of which is closely correlated to a specific physical phenomenon:

$$g_p = g_\mu + g_h + g_m + g_c \quad (32)$$

The structure of the expression of g_p is of a bilinear form: it consists of a summation of two-factor products. The first factor in each term is a flow quantity (heat flow, diffusion flow, momentum flow). The other factor is related to the gradient of an intensive state variable (temperature, chemical potential and velocity gradients).

In the case of fuel cells, an additional term, associated with the entropy generation due to ohmic losses, must be considered in Equation (31):

$$g_{ohm} = \frac{1}{T}\sigma \nabla \varphi \cdot \nabla \varphi \quad (33)$$

This term only appears in the conductive regions, that is, in the electrodes and electrolyte.

When radiation heat transfer is considered, a corresponding entropy generation term must be considered. As in this paper only surface to surface radiation is considered, the specific entropy generation rate refers to the unit surface. Its expression is obtained considering a surface to temperature T that receives radiation from the surrounding emitting surfaces. The infinitesimal emitting surface dA_i is at temperature T_i and the corresponding heat flux is $\vec{J}_{q,rad\ i}$:

$$g_{rad} = \int \vec{J}_{q,rad\ i} \left(\frac{1}{T} - \frac{1}{T_i} \right) \cdot dA_i \quad (34)$$

The local rate of entropy generation due to viscous effects in four longitudinal cross sections [(a) z=20 mm; (b) z=40 mm; (c) z=60 mm; (d) z=80 mm] is depicted in figure 8. The largest values of g_μ are located where there are strong velocity gradients. They take place in a small area near the walls of the air-tube and cathode channel. In addition, viscous effects are also significant in the outlet tube zone; this is related to the presence of vortex structures which increase the viscous stresses. The largest contributions to g_μ are found inside the air-tube and are concentrated in a layer adjacent to the wall tube. The thickness of this layer increases along the cell, due to the development of a velocity boundary layer.

Cite this article as: Sciacovelli A, Verda V, Entropy generation analysis for the design optimization of solid oxide fuel cells International Journal of Numerical Methods for Heat & Fluid Flow Vol. 21 No. 5, 2011 . 535-558, DOI 10.1108/09615531111135819

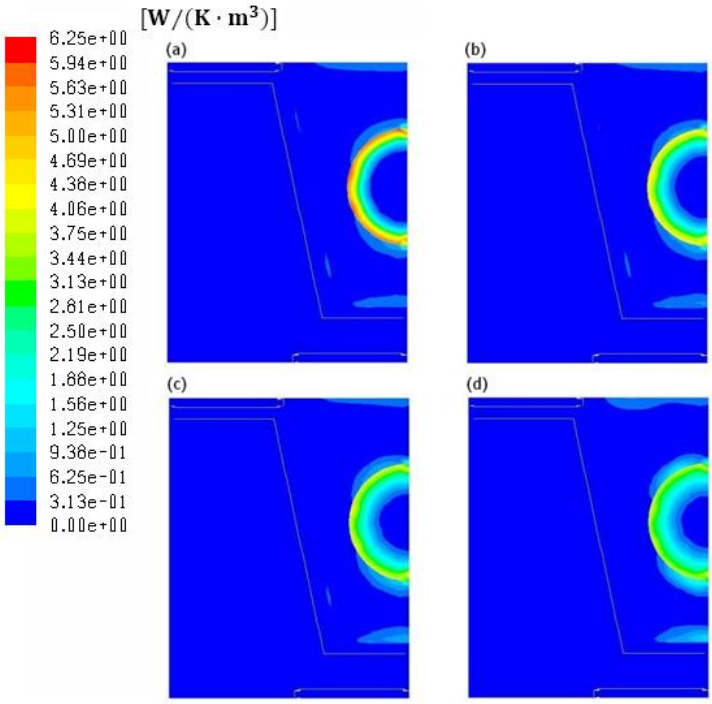

Figure 8. Viscous entropy generation in four cross sections.

The entropy generation due to heat transfer is shown in figure 9. This contribution is mainly found near the electrolyte, where the heat source terms are located. The temperature is lower in the cathode channel than on the fuel side, thus entropy generation is larger. The cross-section plots show that the irreversibility sources at the cathode side increase along the cell. In each cross section, the local maximum value of g_h is located below the air tube where strong temperature gradients can be encountered. The temperature is higher at the anode side, therefore g_h is lower and it decreases along the fuel cell.

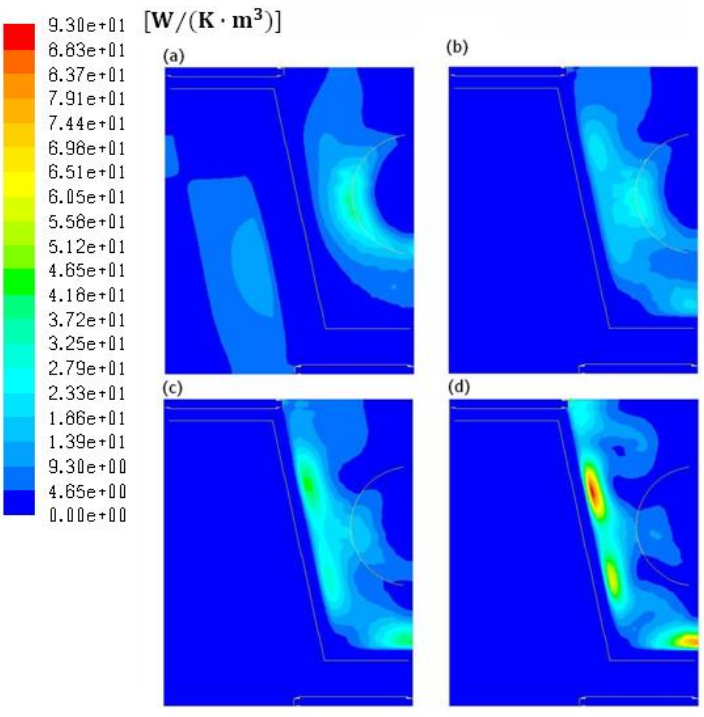

Cite this article as: Sciacovelli A, Verda V, Entropy generation analysis for the design optimization of solid oxide fuel cells International Journal of Numerical Methods for Heat & Fluid Flow Vol. 21 No. 5, 2011 . 535-558, DOI 10.1108/09615531111135819

Figure 9. Entropy generation due to heat transfer on cross section planes.

The contribution to entropy generation from the mass transfer is illustrated in figure 10. The electrochemical reactions cause strong species mass fraction gradients. These gradients are the sources of entropy generation. The irreversibilities are relevant in the porous electrodes, where species motion is driven by diffusion, i.e. species concentration gradients. Large entropy production due to mass transfer is concentrated at the corners of the cell. Moreover, the entropy generation distribution correctly captures where the losses are predominant at the cathode side, i.e. along the upper plane.

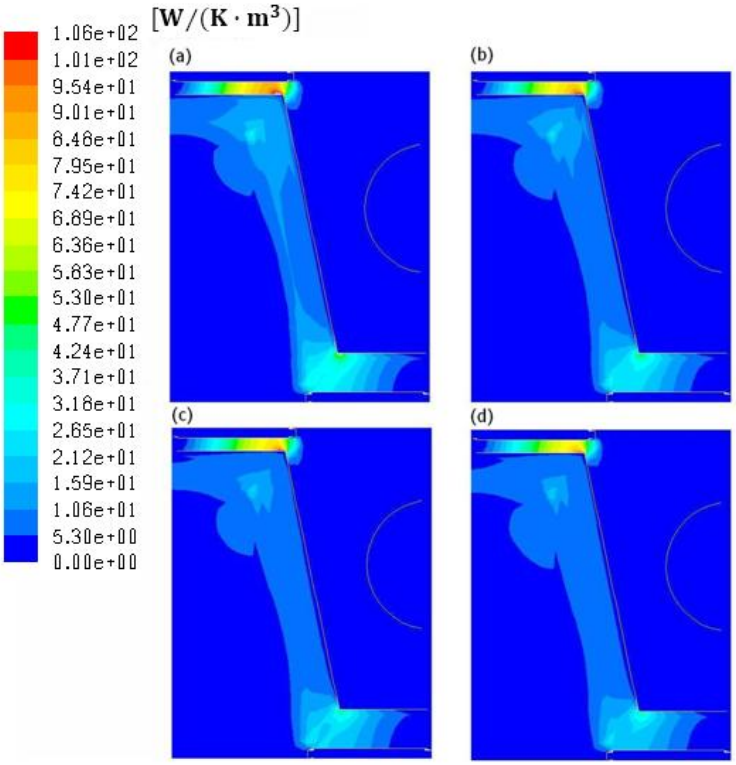

Figure 10. Entropy generation due to mass transfer on cross section planes.

The entropy generated by coupling between heat and mass transfer is depicted in figure 11. This contribution is predominant at the fuel side of the cell, mainly because of strong hydrogen and water mass fraction gradients.

Cite this article as: Sciacovelli A, Verda V, Entropy generation analysis for the design optimization of solid oxide fuel cells International Journal of Numerical Methods for Heat & Fluid Flow Vol. 21 No. 5, 2011 . 535-558, DOI 10.1108/09615531111135819

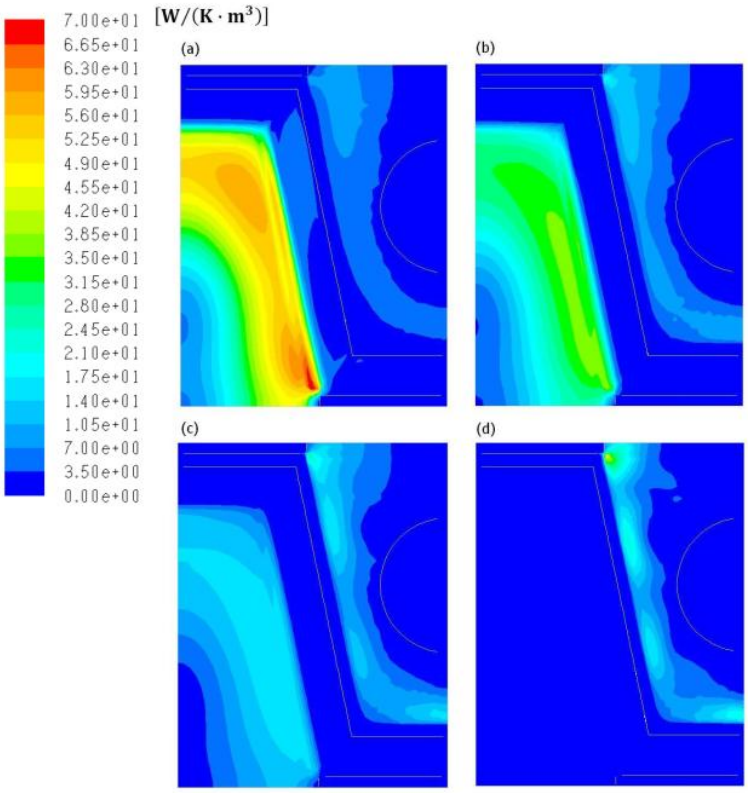

Figure 11. Entropy generation due to coupling between heat and mass transfer.

The last contribution to entropy generation is from the radiation heat transfer. Figure 12 shows the total entropy generation due to the heat transfer, when radiation is considered. As the radiation heat flux is mainly directed from the internal surface of the porous cathode towards the injection tube, the entropy generation term is large on this latter surface. These contributions are discussed in more detail in the next section, where both the local distributions and the global terms are analyzed for optimization purposes.

Cite this article as: Sciacovelli A, Verda V, Entropy generation analysis for the design optimization of solid oxide fuel cells International Journal of Numerical Methods for Heat & Fluid Flow Vol. 21 No. 5, 2011 . 535-558, DOI 10.1108/09615531111135819

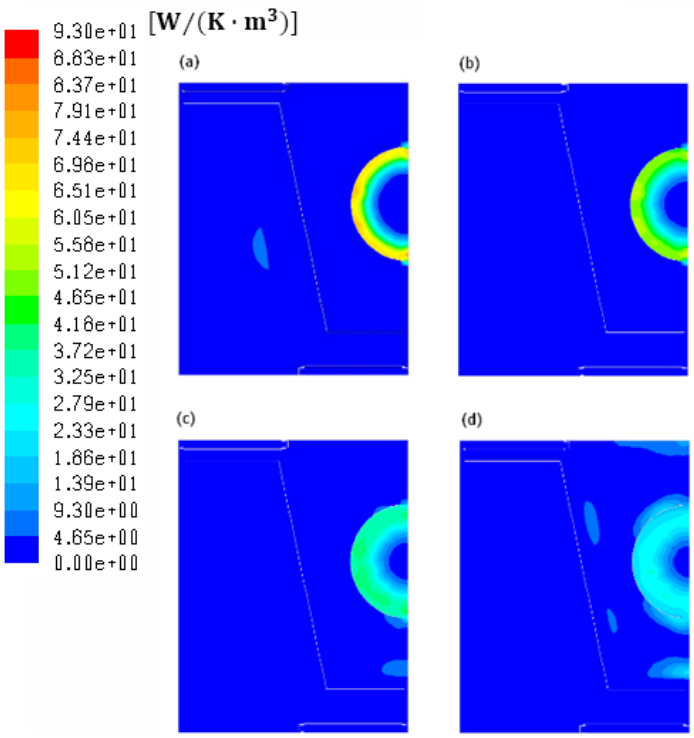

Figure 12. Entropy generation due to heat transfer (including radiation) on cross section planes.

5. GEOMETRY OPTIMIZATION

Optimization has been performed considering the global entropy generation rate as the objective function to minimize, that is:

$$G_p = \int g_\mu + g_h + g_m + g_c + g_{ohm} \cdot dV + \int g_{rad} \cdot dA \qquad (35)$$

Each term in equation (35) is considered separately, in order to understand what the main causes of irreversibility are and to identify the most appropriate design variables (i.e. the independent variables) to use in the optimization. Figure 13 shows the five contributions to the global entropy generation, when radiation is considered or not considered. The contribution due to radiation heat transfer is the largest, which means that when radiation is not considered, we not only obtain a different temperature distribution but also neglect the main cause of the irreversibilities. When the radiation heat transfer is not considered, the main contribution to the global entropy generation is due to coupling between the heat and mass transfer, i.e. the temperature gradients associated with convection. Therefore, if radiation is neglected we first try to reduce the convective term to optimize the cell, while if the radiation is considered we first try to reduce the radiation heat transfer.

Cite this article as: Sciacovelli A, Verda V, Entropy generation analysis for the design optimization of solid oxide fuel cells International Journal of Numerical Methods for Heat & Fluid Flow Vol. 21 No. 5, 2011 . 535-558, DOI 10.1108/09615531111135819

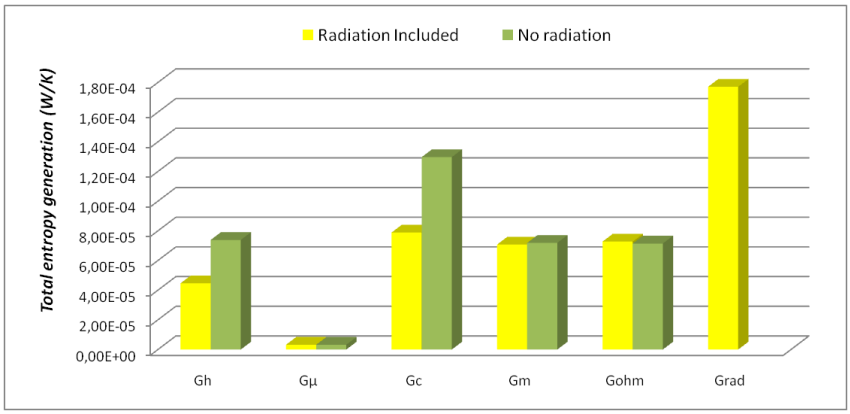

Figure 13. Global contributions to the entropy generation

The tube diameter is considered as a design variable in order to reduce the radiation between the cathode and the tube. Figure 14 shows the effect of the injection tube diameter on the power density. It can be observed how power density increases with reducing diameter. When the diameter becomes smaller than 3.5 mm, the increase in power density reduces. The reason for this is that a significant increase in the contribution occurs due to viscous effects. Below 2.5 mm, a level which is not represented in the figure, viscous effects cause a reduction in power density.

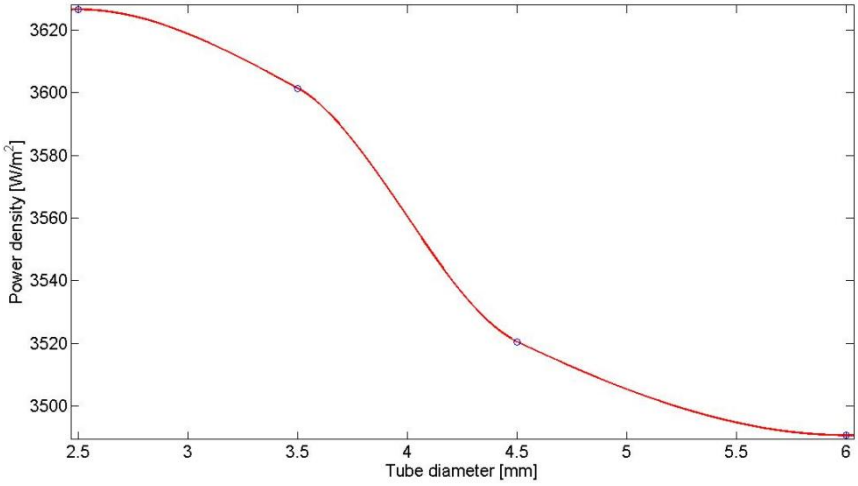

Figure 14. Effect of tube diameter on power density.

Other important contributions to the entropy generation are those associated with mass transfer: pure mass transfer and coupling between the heat and mass transfer. In order to reduce these contributions, it is possible to operate letting the shape of the fuel cell free to vary. To this aim, the SOFC geometry is parameterized using two scaling factors: along *x* and *y*. These factors are defined as the ratio between a dimension of the fuel cell in the current design and the dimension in the initial design.

Once we have identified the contribution to the entropy generation that should be reduced, it is important to reduce its picks. The scaling factor along y is expected to have an effect on the entropy generation due to the coupling between the heat and mass transfer and the entropy generation due the mass transfer. These picks are the highest (see Figures 10 and 11), thus the effect that should be obtained by modifying this parameter is expected to be large. In particular, when this value is reduced compared to the initial design, it is expected that entropy generation will decrease. The scaling factor along x mainly affects the entropy generation due to heat transfer, reducing a pick on the anodic side (see Figure

Cite this article as: Sciacovelli A, Verda V, Entropy generation analysis for the design optimization of solid oxide fuel cells International Journal of Numerical Methods for Heat & Fluid Flow Vol. 21 No. 5, 2011 . 535-558, DOI 10.1108/09615531111135819

9) when it is increased compared to the initial design. In the optimization procedure, the total active surface has been constrained to a fixed value. Thus, the total TPB sites for electrochemical reactions are constant for all the examined geometries. This means that the scaling factor along z is obtained from the values of the two other scaling factors, together with the constraint on the active surface.

The SIMPLEX algorithm is used to perform the optimization as it is a single objective function problem (see, for example, Rao, 1996). The optimization process involves the following steps: the optimization algorithm generates a set of numbers, i.e. the geometrical design variables, that represent the fuel cell shape. These parameters are sent to the mesh generator which creates and passes the computational grid to the CFD solver. This solver computes the conservation equations and the objective function that have to be minimized. Finally, the numerical values of the objective functions are sent back to the optimizer, which generates a new case, and so on.

A bubble chart is shown in Figure 15. This representation is used since the data have third and fourth dimensions that need to be shown on the same chart. In this case, the x and y scaling factor are reported along the abscissa and ordinate, and the diameter of the bubble indicates the z scaling factor. Finally, the color map shows the global entropy generation in the fuel cell. This chart confirms that the effect on the total entropy generation obtained through changes in the y scaling factor is the largest.

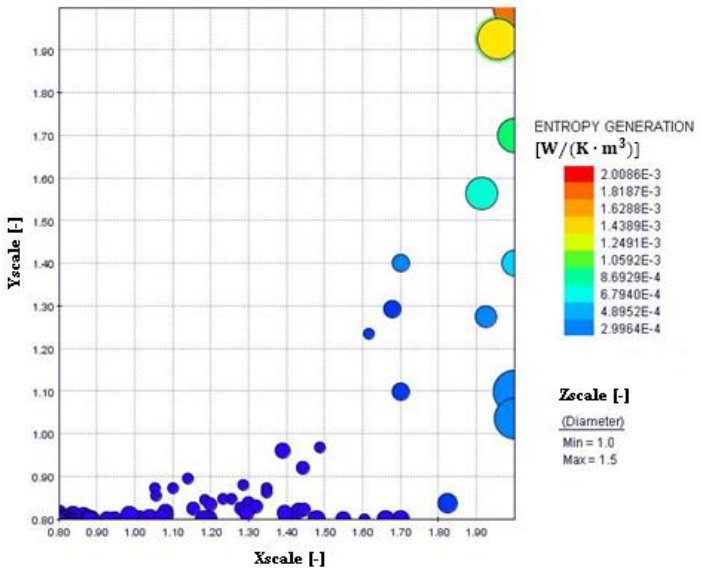

Figure 15. Bubble chart of entropy generation.

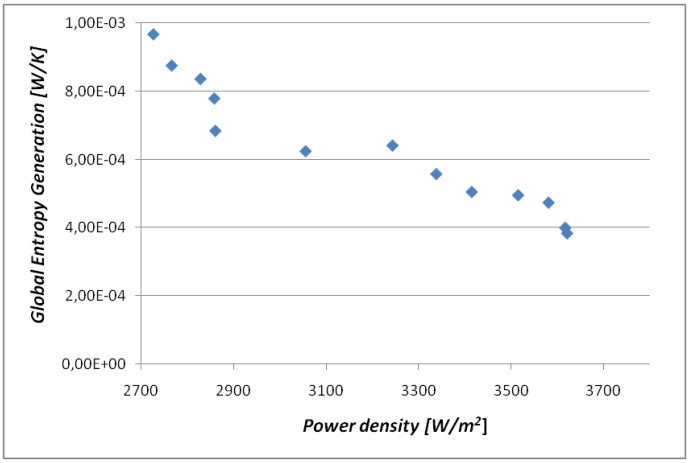

Cite this article as: Sciacovelli A, Verda V, Entropy generation analysis for the design optimization of solid oxide fuel cells International Journal of Numerical Methods for Heat & Fluid Flow Vol. 21 No. 5, 2011 . 535-558, DOI 10.1108/09615531111135819

Figure 16. Entropy generation vs. Power density.

Various geometries analyzed during the optimization process are considered in Figure 16. The figure shows that a reduction in the entropy generation leads to an increase in the electric power produced per unit active area (i.e. an increase in the current density, as the operating voltage is fixed). This is particularly important as power density is one of the main parameters that can reduce the fuel cell investment costs.

The optimal configuration is obtained for the X scale = 1.4 and the Y scale = 0.8, which means that the optimal length in the y direction is smaller than in the initial design, while the length in the x scale is larger. This shape allows one to reduce the fluid flow resistances towards the active surface, in correspondence to the upper edge, where the entropy generation due to mass transfer presents high picks. Figure 17 shows that the picks in the optimal design are significantly reduced.

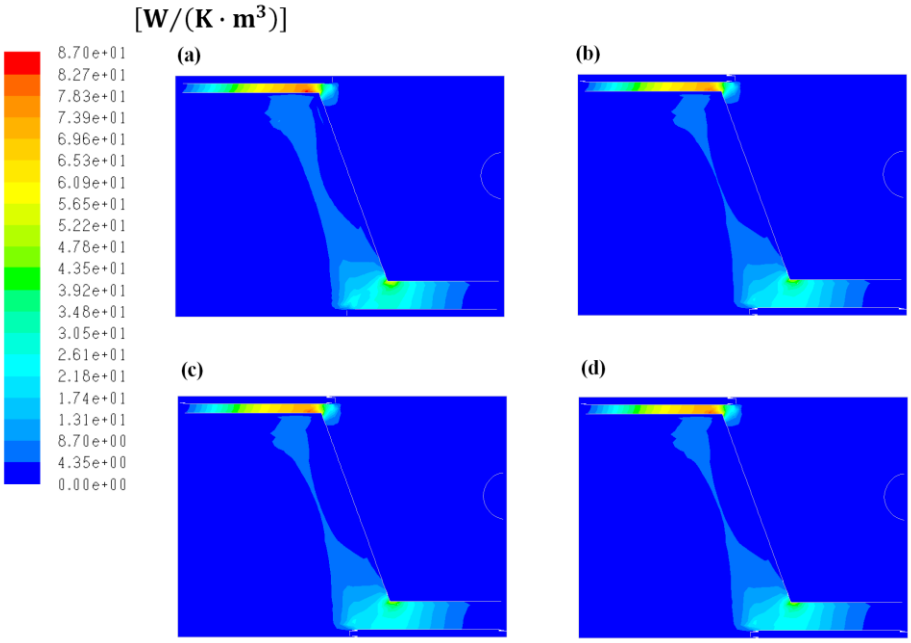

Figure 17. Entropy generation due to mass transfer in the optimal design.

Compared with the initial design, in the optimal configuration the contributions to the global entropy generation due to radiation heat transfer and to mass transfer reduce. The contributions due to ohmic heating and coupling between heat and mass transfer increase because of the increased current density, thus these are not negative effects. A comparison between the initial design and the optimal design is presented in Figure 18.

Cite this article as: Sciacovelli A, Verda V, Entropy generation analysis for the design optimization of solid oxide fuel cells International Journal of Numerical Methods for Heat & Fluid Flow Vol. 21 No. 5, 2011 . 535-558, DOI 10.1108/09615531111135819

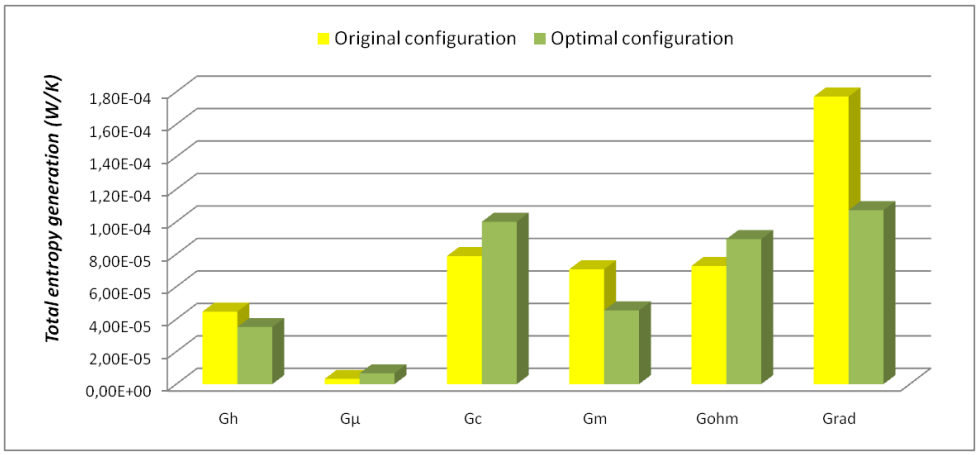

Figure 18. Global contributions to the entropy generation in the initial design and in the optimal configuration

Together with costs, another important technical parameter which should be considered is the volume of the device. Figure 19 shows some results obtained by performing the optimization using the power density as the objective function to be maximized. On the left side of the diagram, it is possible to notice that a small reduction in the power density (from about 3640 W/m^2 to about 3615 W/m^2) allows a significant reduction in the fuel cell volume, of about 20%.

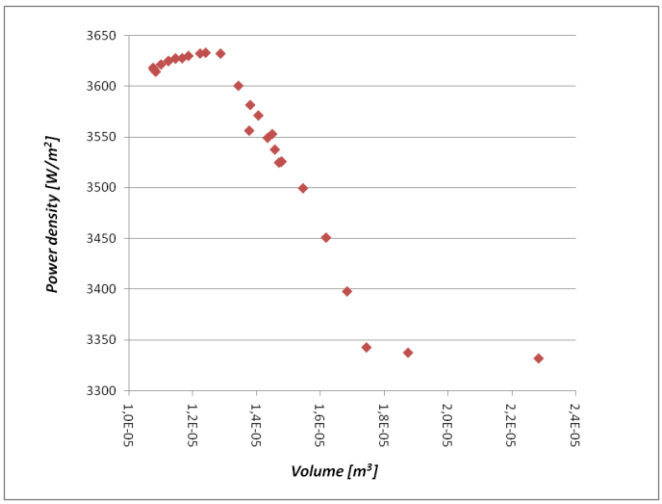

Figure 19. Fuel cell volume for various designs

5. CONCLUSIONS

The optimization of the geometry of a tubular solid oxide fuel cell has been conducted in this paper using the minimum entropy generation as the objective function.

The separate contributions to the entropy generations have also been calculated: heat transfer, viscous flow, coupling between the heat and mass transfer, diffusive term, and current transfer. In addition, as radiation heat transfer has been considered in the model, the impact of this term on the entropy generation has been evaluated. It has been shown that this entails the largest contribution to the total entropy generation, thus it is particularly important to consider this term as it has a strong impact on the temperature profiles as well as the fuel cell performances.

Cite this article as: Sciacovelli A, Verda V, Entropy generation analysis for the design optimization of solid oxide fuel cells International Journal of Numerical Methods for Heat & Fluid Flow Vol. 21 No. 5, 2011 . 535-558, **DOI 10.1108/09615531111135819**

The choice of the design parameters has been made on the basis of values assumed for the various contributions to the total entropy generation. In particular, the injection tube diameter has been selected as it affects the entropy generation due to radiation heat transfer. The scaling factors are considered as they affect the contributions to the conduction and to convection heat transfer.

With respect to the initial design, the entropy generation in the optimized geometry is reduced by about 25%, while the power density is increased by about 10%. Another benefit that can be achieved in the optimization concerns the fuel cell volume. As this may be an issue in the design process, it is worth considering a multi-objective optimization, assuming entropy generation and volume as the two objective functions.

REFERENCES

Andersson M, Yuan J, Sundén B. (2010). "Review on modeling development for multiscale chemical reactions coupled transport phenomena in solid oxide fuel cells". Applied Energy 87: 1461–1476

Arpino F., Massarotti N. (2009). "Numerical simulation of mass and energy transport phenomena in solid oxide fuel cells", Energy, 34, pp. 2033–2041

Bejan A. (1982). "Entropy Generation through Heat and Fluid Flow", Wiley, New York, NY.

Bird R.B., Steward W.E., Lightfoot E.N. (1960), "Transport Phenomena", J. Wiley & Sons, New York

Calì M., Santarelli M.G.L., Leone P. (2006), "Computer experimental analysis of the CHP performance of a 100kWe SOFC Field Unit by a factorial design", Journal of Power Sources, 156, pp. 400–413.

Chan, S.H., Khor, K.A. and Xia, Z.T. (2001), "A complete polarization model of a solid oxide fuel cell and its sensitivity to the change of cell components thickness", *Journal of Power Sources*, Vol. 93, pp. 130–40.

Chui E. H. and Raithby G. D., "Computation of Radiant Heat Transfer on a Non-Orthogonal Mesh Using the Finite-Volume Method," *Numerical Heat Transfer, Part B*, Vol. 23, pp. 269-288, 1993.

Costamagna, P., Selimovic, A., Del Borghi, M. and Agnew, G. (2004) "Electrochemical model of the integrated planar solid oxide fuel cell IP-SOFC", *Chemical Engineering Journal*, Vol. 102, pp. 61–9.

Damm D., and Fedorov, G. (2005), "Radiation heat transfer in SOFC materials and components", *Journal of Power Sources*, Vol. 143, pp. 158–165.

Fischer K, Seume J. (2006). "Location and magnitude of heat sources in solid oxide fuel cells". In: Proceedings of FUELCELL2006.

Fuller E.N., Schettler P.D., Giddings J.C. (1966). A new method for prediction of binary gas-phase diffusion coefficients. Industrial and Engineering Chemistry. 58, 5; 18-27.

Haynes, C. and Wepfer, WJ. (2001), "Characterizing heat transfer within a commercial-grade tubular solid oxide fuel cell for enhanced thermal management", Int. J of Hydrogen Energy, 26, pp. 369-379.

Hirschfelder, J. O., Curtiss, C. F. and Bird, R. B. (1954), Molecular Theory of Gases and Liquids, Wiley, New York, NY.

Hwang J.J., Chen C.K., Lai D.Y. (2005) "Computational analysis of species transport and electrochemical characteristics of a MOLB-type SOFC". Journal of Power Sources 140: 235–242.

Kakaç S., Pramuanjaroenkij A., Zhou X.Y. (2007). "A review of numerical modeling of solid oxide fuel cells", Int. J of Hydrogen Energy, 32, pp. 761 – 786.

Cite this article as: Sciacovelli A, Verda V, Entropy generation analysis for the design optimization of solid oxide fuel cells International Journal of Numerical Methods for Heat & Fluid Flow Vol. 21 No. 5, 2011 . 535-558, **DOI 10.1108/09615531111135819**

Krishna, R. and Wesselingh, J. A. (1997), "The Maxwell-Stefan approach to mass transfer". Chemical Engineering Science, 52, pp. 861-911.

Larminie J., Dicks A. (1999). "Fuel cell systems explained". Wiley.

Li P., Chyu M.K. (2003). Simulation of the chemical/electrochemical reactions and heat/mass transfer for a tubular SOFC in a stack. Journal of Power Sources. 124; 487–498

Li P.W., Suzuki K. (2004), "Numerical modeling and performance study of a tubular SOFC". Journal of the Electrochemical Society, 151, pp. A548-A557.

Modest, M.F. (2003), *Radiative Heat Transfer*, 2nd ed. Academic Press, New York, NY.

National Energy Technology Laboratory, U.S. Department of Energy (2004). Fuel Cell Handbook. Available at: http://www.netl.doe.gov

Nield D.A., Bejan A. (1999), "Convection in porous media", New York: Springer.

Noren, D.A. and Hoffman, M.A. (2005), "Clarifying the Butler–Volmer equation and related approximations for calculating activation losses in solid oxide fuel cell models", *Journal of Power Sources*, Vol. 152, pp. 175–181

Ota, T., Koyama, M., Wen, C., Yamada, K. and Takahashi H (2003) "Object-based modeling of SOFC system: dynamic behavior of micro-tube SOFC". Journal of Power Sources, 118, pp. 430-439.

Patankar, S.V. (1980). "Numerical heat transfer and fluid flow". Hemisphere. Washington DC

Rao, S.S. (1996). "Engineering Optimization: Theory and Practice", 3rd Edition. John Wiley and Sons.

Sciacovelli, A. and Verda, V. (2008). "Entropy generation minimization in a tubular solid oxide fuel cell". ASME paper IMECE2008-68910. Proceedings of IMECE 2008, Boston, Massachusetts, October 31 - November 6.

Sciacovelli A., Verda V. (2009) Entropy generation analysis in a monolithic-type solid oxide fuel cell (SOFC). Energy 34. 850-865.

Various Authors (2008). "Modeling Solid Oxide Fuel Cells. Method, Procedures and Techniques". R. Bove and S. Ubertini Editors. Springer.

Various Authors (2005). "Solid Oxide Fuel Cells IX". Singhal S.C. and Mizusaki J. Editors. The Electrochemical Society.

Verda V., Borchiellini R. (2007) "Performance Analysis of Solid Oxide Fuel Cell Stack. Part 2: Radiation Heat Transfer Model". ASME IMECE 2007. Seattle, U.S.A.

Yakabe H., Hishinuma M., Uratani M., Matsuzaki Y., Yasuda I. (2000). Evaluation and modeling of performance of anode-supported solid oxide fuel cell. Journal of Power Sources. 86; 423–431

Yang Y., Wang G., Zhang H., Xia W. (2007). Computational analysis of thermo-fluid and electrochemical characteristics of MOLB-type SOFC stacks. Journal of Power Sources 173, pp. 233–239.